CHAPTER III

MEASUREMENTS OF VOLUME FRACTIONS IN TWO-PHASE AND THREE-PHASE FLUIDIZED BEDS

3.1 Introduction

X-ray and γ-ray densitometers have been used to measure porosities of fluidized beds (Miller and Gidaspow, 1993; Gidaspow, et al., 1983) and solids concentrations in nonaqueous suspensions (Jayaswal, et al., 1990). These techniques are based on the fact that the gas, liquid and solid phases under consideration have different absorptivities for x-rays and γ-rays. The same concept was adopted to measure concentration profiles inside our three-phase (air-water-lead glass bead) fluidization systems.

3.2 Principle of Interpretation

The absorption of x-ray or γ-ray by any material depends mainly on the molecular weight of the material. The amount of radiation that is absorbed by a material can be explained by the Beer-Bourget-Lambert Law :

$$I = I_o \exp(-\kappa \rho l) \qquad (3.1)$$

where I is the Intensity of transmitted radiation, I_o the intensity of incident radiation, κ is the attenuation coefficient, ρ the density of material, and l is the path length. The attenuation coefficient is calculated from a calibrated curve. The logarithmic form of equation (3.1) is :

$$\ln\left(\frac{I_o}{I}\right) = A \qquad (3.2)$$

where A= κρl.

For a mixture of n phases, the intensity of the transmitted X-rays or γ-rays could be described as a linear function of the volume fractions of the phases as :

$$\ln\left(\frac{I}{I_o}\right) = A_1\epsilon_1 + A_2\epsilon_2 + \ldots + A_n\epsilon_n \qquad (3.3)$$

where ϵ_n is the volume fraction of phase n. The transmitted energy of radiation from both densitometers was placed into logarithmic form.

Another relation for ϵ_n is :

$$\epsilon_1+\epsilon_2+\ldots+\epsilon_n = 1 \qquad (3.4)$$

For three-phase fluidized beds, there are three unknowns, volume fraction of gas (ϵ_g), volume fraction of liquid (ϵ_l), and volume fraction of solid (ϵ_s). In order to estimate the unknowns, the equations (3.3) and (3.4) are simplified to form the following three equations :

$$\ln\left(\frac{I_X}{I_{o,X}}\right) = A_{g,X}\,\epsilon_g + A_{l,X}\,\epsilon_l + A_{s,X}\,\epsilon_s \qquad (3.5)$$

$$\ln\left(\frac{I_\gamma}{I_{o,\gamma}}\right) = A_{g,\gamma}\,\epsilon_g + A_{l,\gamma}\,\epsilon_l + A_{s,\gamma}\,\epsilon_s \qquad (3.6)$$

$$\epsilon_g + \epsilon_l + \epsilon_s = 1 \qquad (3.7)$$

where I_X and I_γ are the intensity readings of X-ray and γ-ray densitometers.

3.3 Calibration of X-ray and γ-ray Densitometer

Before any measurements of the gas, liquid and solids concentration during the fluidization could be made, the x-ray and γ-ray densitometers had to be calibrated for the system. The coefficients in equations (3.5) and (3.6) were statistically calculated using the least square error technique from the calibration measurements of the intensity readings of X-ray and γ-ray densitometers at known concentrations of gas, liquid and solids in three-phase mixtures. However, these coefficients were found to have values with 20% of error for X-ray and 2% of error for γ-ray. The complete calibration curves for both X-ray and γ-ray in a three-phase fluidized bed were obtained using the following calibrated mixtures :

a. Gas :

$\varepsilon_g = 1.0, \varepsilon_l = 0.0, \varepsilon_s = 0.0$

b. Gas-Solid packed :

$\varepsilon_g = (1.0 - \varepsilon_{s,max}), \varepsilon_l = 0.0, \varepsilon_s = \varepsilon_{s,max}$

c. Liquid-Solid :

$\varepsilon_g = 0.0$, ε_l, ε_s = a range of average volume fractions values based on visual observations of initial and fluidized bed heights, including,

c-1. Liquid :

$\varepsilon_g = 0.0, \varepsilon_l = 1.0, \varepsilon_s = 0.0$

c-2. Liquid-solid packed:

$\varepsilon_g = 0.0, \varepsilon_l = (1.0 - \varepsilon_{s,max}), \varepsilon_s = \varepsilon_{s,max}$

Typical linear calibration curves for the liquid-solid (water-lead glass beads) system for x-ray and γ-ray densitometers are shown in the Figures 3.1 and 3.2, respectively. Each point in the plot represents an average of 15-20 readings of the intensity of the x-ray or γ-ray transmitted through the bed.

To obtain the time averaged volume fractions at a designated position inside the three-phase fluidized bed, an integration time of 40 seconds was used. The x-ray and γ-ray densitometers intensities through the bed were obtained. From the calibration curves, the time average values of volume fractions for gas, liquid and solid phases were computed.

3.4 Results and Discussion

3.4.1 Flow Regime. Three different flow regimes normally occur in three phase fluidized beds : the coalesced bubble, the dispersed bubble, and the slugging regimes (Fan, 1989). Figure 3.3 shows a typical flow regime map (Deckwer et al., 1980) for a liquid-batch bubble column or a slurry-batch slurry bubble column containing a low viscosity liquid phase.

Figure 3.4 shows a typical photograph of the three-phase fluidization experiment. The experimental conditions are shown in the Table 2.1. The superficial velocities for gas and liquid phases were 3.37 cm/sec and 2.03 cm/sec, respectively. As seen in Figure 3.4, three distinct bubbles of about 3.0 cm diameter are visible on the bottom left, bottom right and top center of the bed. As reported in Chapter 2, the mean bubble diameter at the time of its release from the gas distributor was only 0.124 mm. Thus, the two-

dimensional three phase fluidized bed was operating in the coalesced bubble regime, which was due to a low superficial liquid velocity and a high superficial gas velocity. The gas bubbles formed on both sides of the bed, moved towards the center and coalesced together forming bigger bubbles. The bigger bubbles moved upwards through the bed with a larger velocity.

Bouillard and Gidaspow (1991) have shown that in a gas-solid fluidized bed, when the gas at the bottom moves faster than in the rest of the bed, there is a catch-up effect and large gas voids may form. It is the packing effect of the bubbles that produces this regime. When the injected bubbles are far apart, for low gas velocities, the bubbles move up at constant velocities, as in a dispersed flow regime. However, at high gas velocities, the gas volume fraction is high. Here the paths of the small injected bubbles intersect and the bubbles coalesce. The situation is similar to that described in chapter 6 for gas-solid fluidized beds by Gidaspow (1994).

The flow regimes for concurrent air-water-particle fluidized beds have been mapped out by Muroyama and Fan (1989) in terms of gas and liquid superficial velocities. Based on the experimental operating conditions, Figure 3.5 (Muroyama and Fan, 1985) also shows that the flow regime is the coalesced bubble regime.

3.4.2 Volume Fractions. The experimental volume fraction measurements were made at 240 different locations at every 1.27 cm in both x and y directions on the left portion of the bed as shown in Figure 3.6. Figures 3.7(a) to 3.7(c) show the experimental results for the time-averaged volume fractions of gas, liquid and solid, respectively.

Figures 3.7(b) and 3.7(c) show that there exists a region of a maximum value of

time averaged volume fraction of gas, slightly shifted away from the center line, that has a value of approximately 0.7. This region can be interpreted as a region through which most of the coalesced bubbles pass. Figures 3.7(a) and 3.7(c) show that there are solids close to the wall. This is due to the downward flow of the gas and the liquid near the wall, causing the solids to entrain and move down in that region.

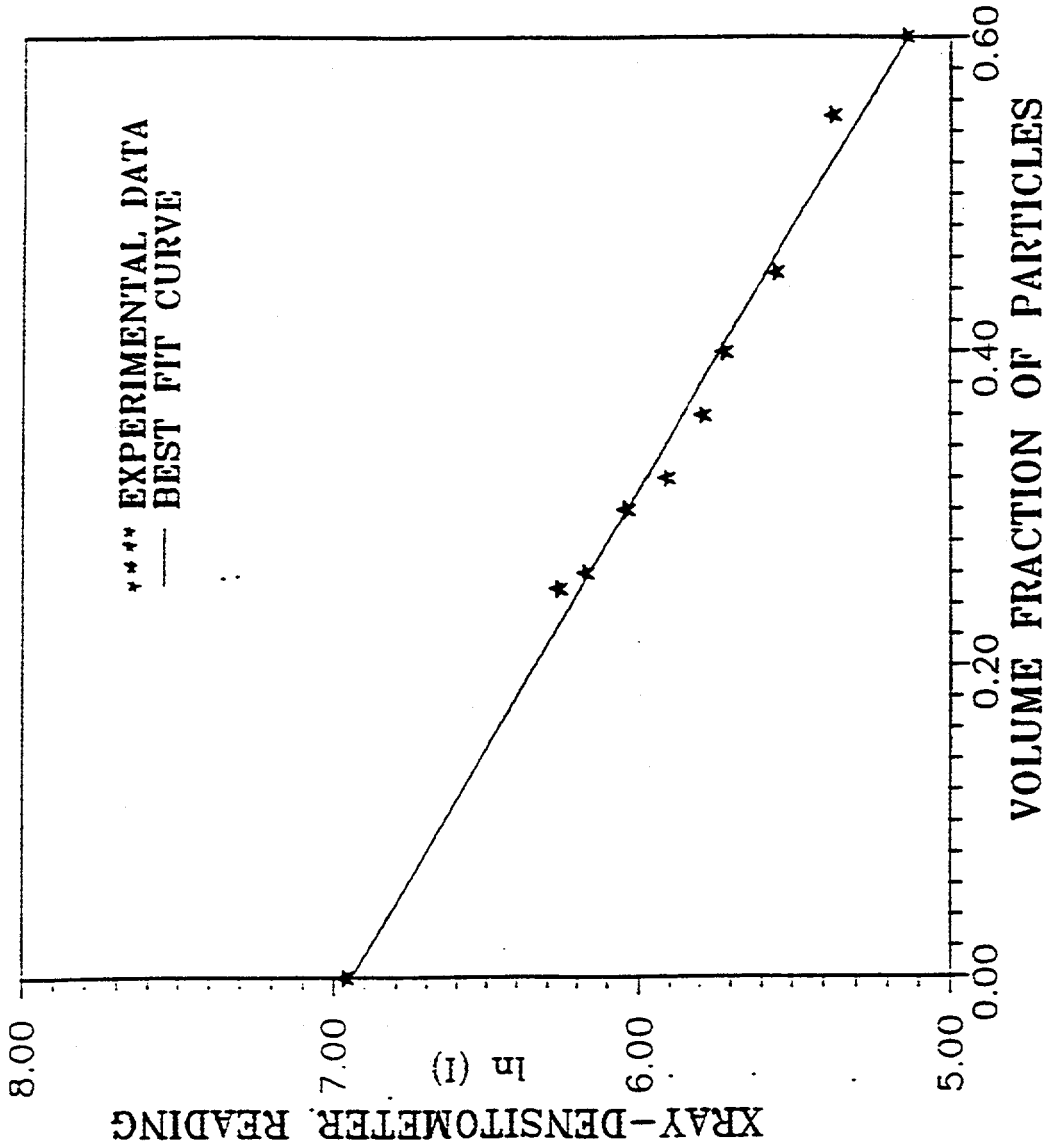

Figure 3.1. An x-Ray Calibration Curve for Lead Glass Beads

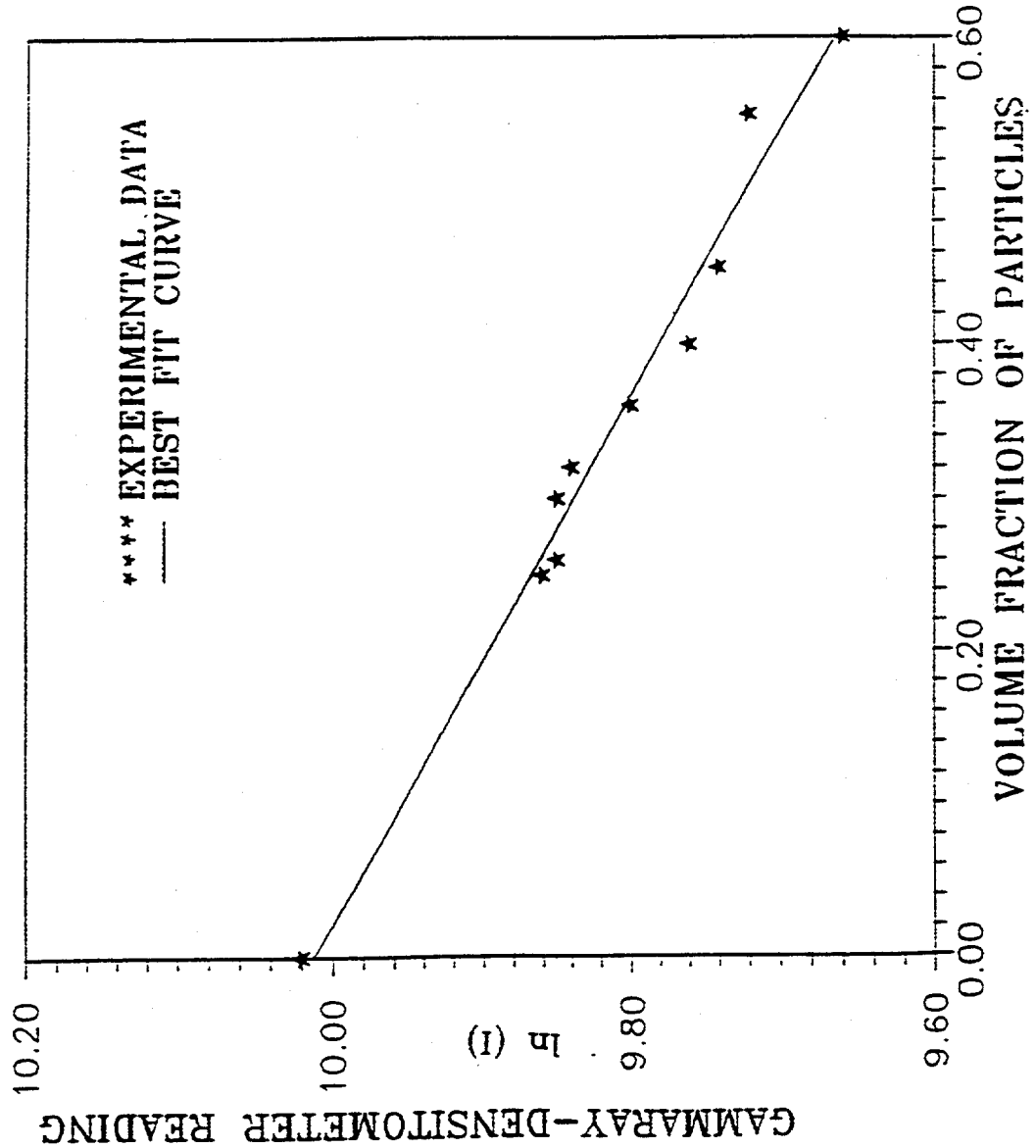

Figure 3.2. A g-Ray Calibration Curve for Lead Glass Beads

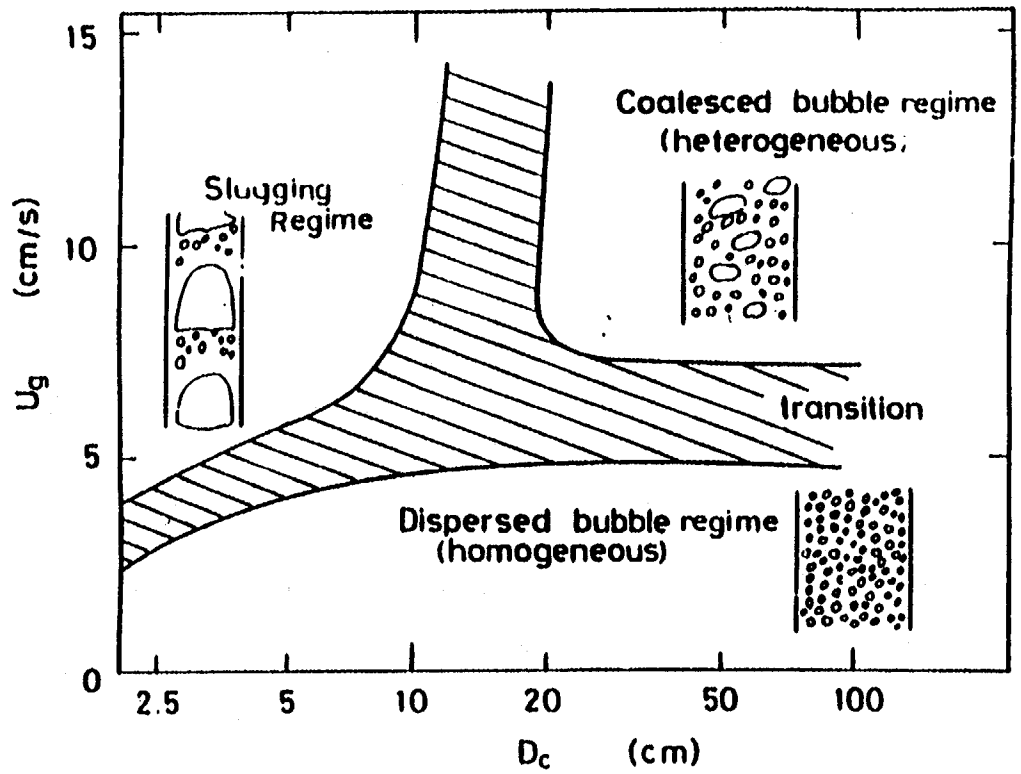

Figure 3.3. Flow Regime Map for a Liquid-batch Bubble Column or a Slurry-batch Slurry Bubble Column Containing a Low Viscosity Liquid Phase (from Deckwer et al. 1980)

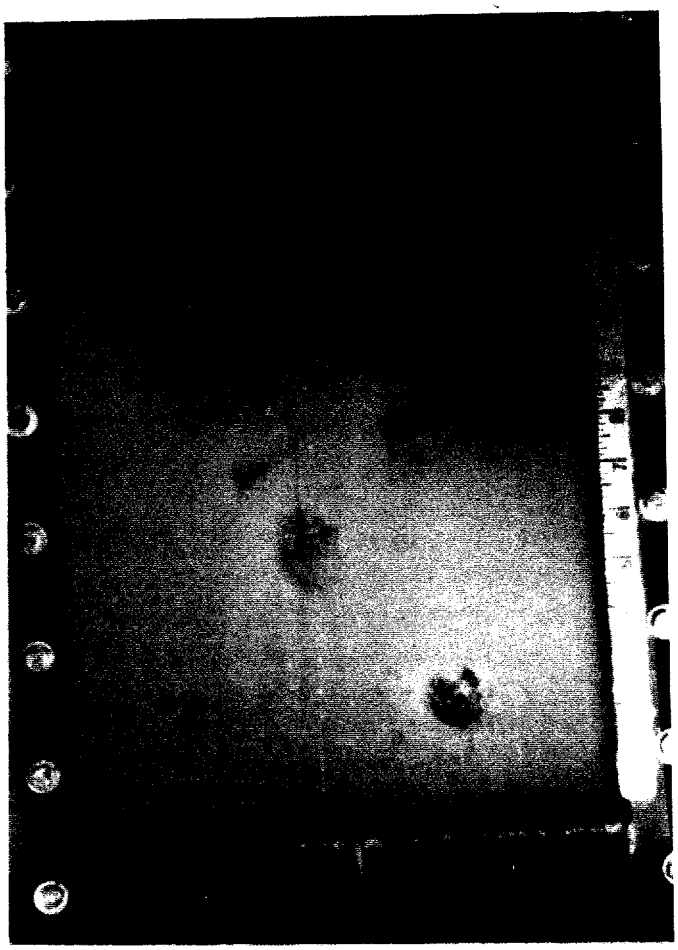

Figure 3.4. Photograph of Coalescence Regime in a Gas-Liquid-Solid Fluidized Bed, with Uniform Liquid and Gas Injection

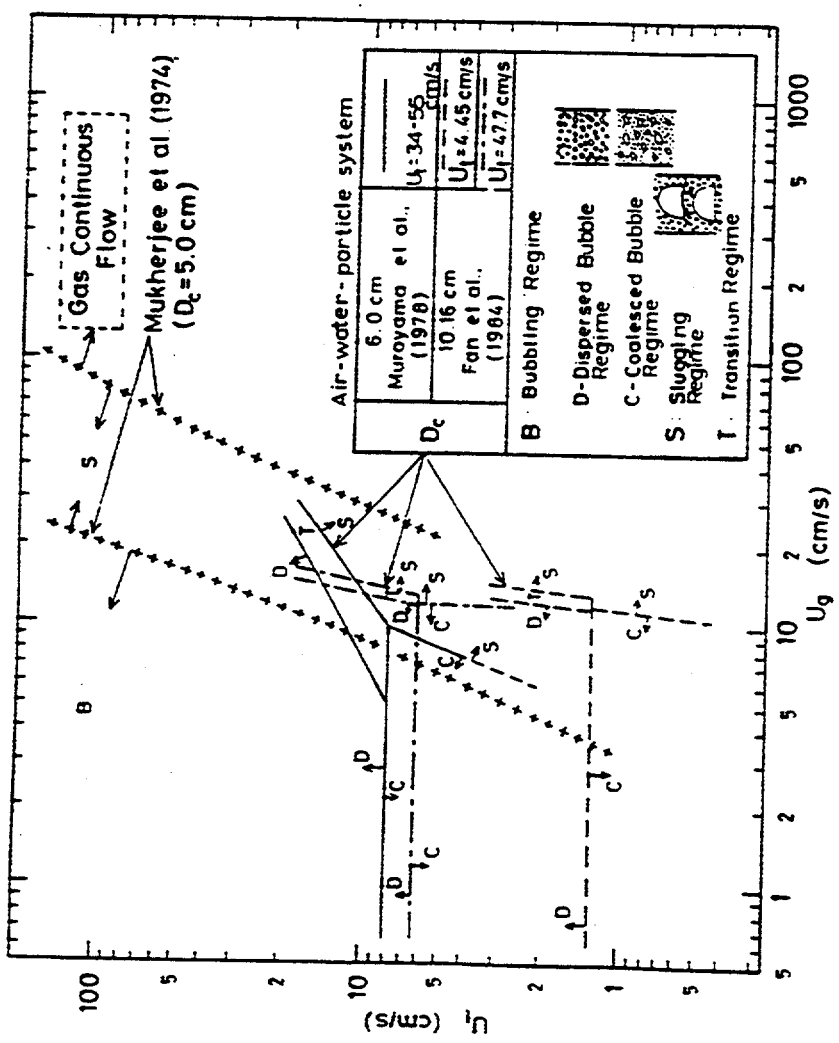

Figure 3.5. Flow Regime Diagram for Cocurrent Gas-Liquid-Solid Fluidized Beds (from Muroyama and Fan, 1985)

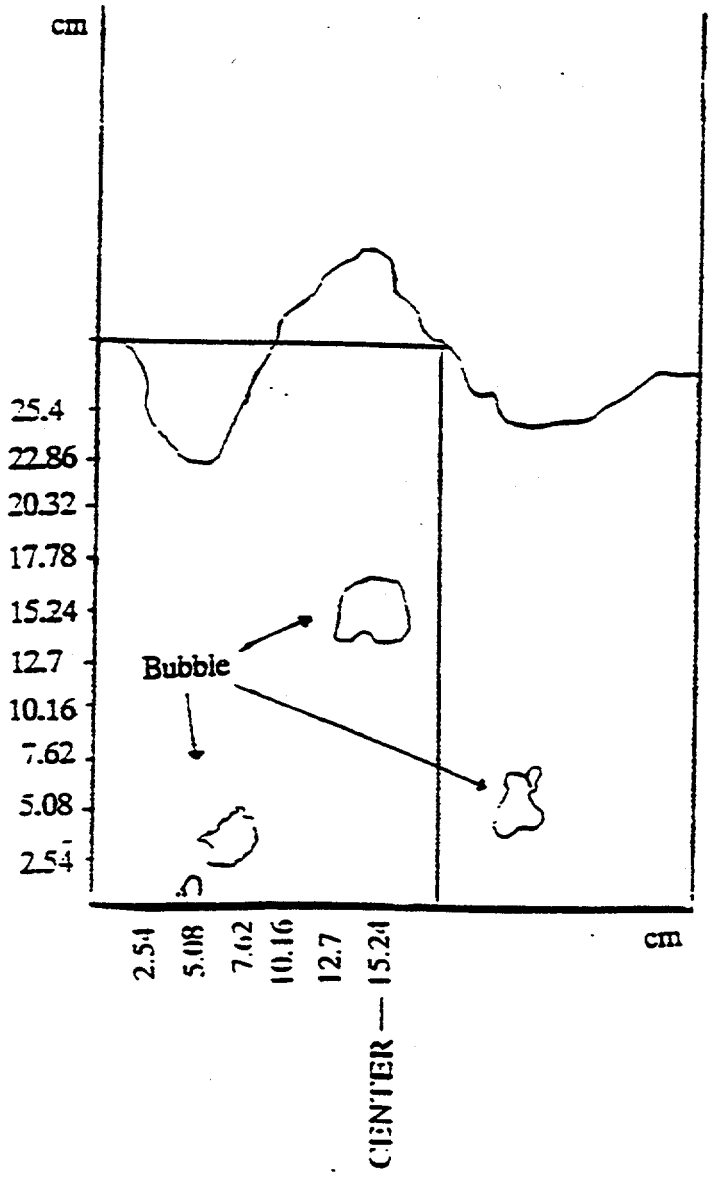

Figure 3.6. The Portion of The Bed Where Measurements Were Obtained

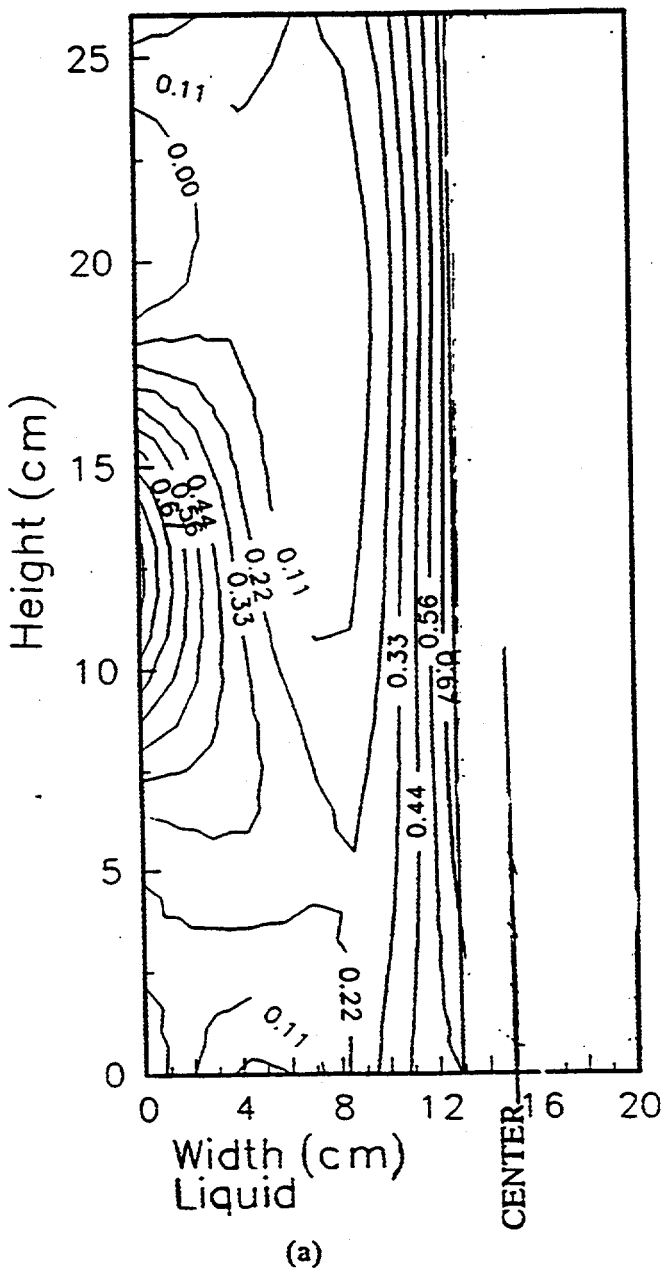

(a)

Figure 3.7(a). Experimental Time Average Volume Fraction Contours for liquid

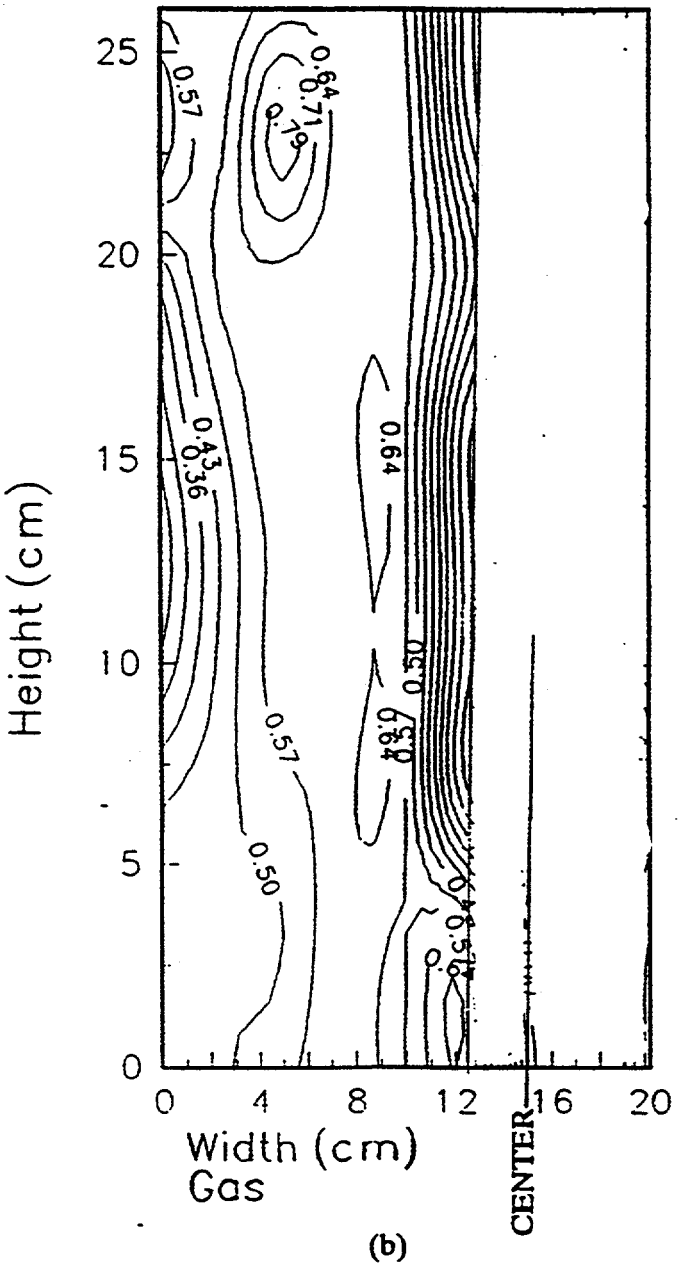

Figure 3.7(b). Experimental Time Average Volume Fraction Contours for Gas

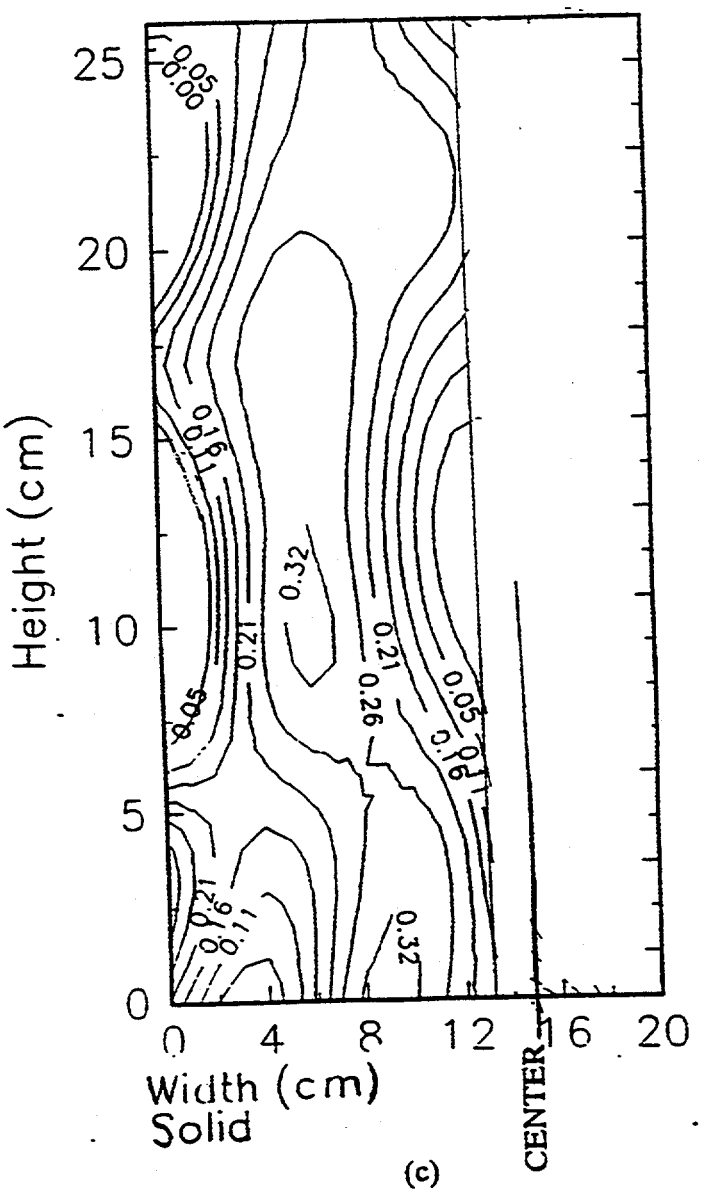

Figure 3.7(c). Experimental Time Average Volume Fraction Contours for Solid